ACS APPLIED MATERIALS & INTERFACES

Research Article

www.acsami.org

Using Three-Dimensional 3D Grazing-Incidence Small-Angle X-ray Scattering (GISAXS) Analysis To Probe Pore Deformation in Mesoporous Silica Films

Elvia Anabela Chavez Panduro,[†,‡] Håvard Granlund,[§] Michael Sztucki,[‡] Oleg Konovalov,[‡] Dag W. Breiby,*[,§] and Alain Gibaud*[,†]

[†]LUNAM, UMR CNRS 6283, Université du Maine, Faculté des Sciences et Technologie, Bd O. Messiaen, 72085 Le Mans, Cedex 09, France

[‡]European Synchrotron Radiation Facility, BP 220, 38043 Grenoble Cedex, France

[§]Department of Physics, Norwegian University of Science and Technology, Høgskoleringen 5, 7491 Trondheim, Norway

Supporting Information

ABSTRACT: In the past decade, remarkable progress has been made in studying nanoscale objects deposited on surfaces by grazing-incidence small-angle X-ray scattering (GISAXS). However, unravelling the structural properties of mesostructured thin films containing highly organized internal three-dimensional (3D) structures remains a challenging issue, because of the lack of efficient algorithms that allow prediction of the GISAXS intensity patterns. Previous attempts to calculate intensities have mostly been limited to cases of two-dimensional (2D) assemblies of nanoparticles at surfaces, or have been adapted to specific 3D cases. Here, we demonstrate that highly organized 3D mesoscale structures (for example, porous networks) can be modeled by the combined use of established crystallography formalism and the Distorted Wave Born Approximation (DWBA). Taking advantage of the near-zero intensity of symmetry-allowed Bragg reflections, the casual extinction or existence of certain reflections related to the anisotropy of the form factor of the pores can be used as a highly sensitive method to extract structural information. We employ this generic method to probe the slightly compressed anisotropic shape and orientation of pores in a mesoporous silica thin film having $P6_3/mmc$ symmetry.

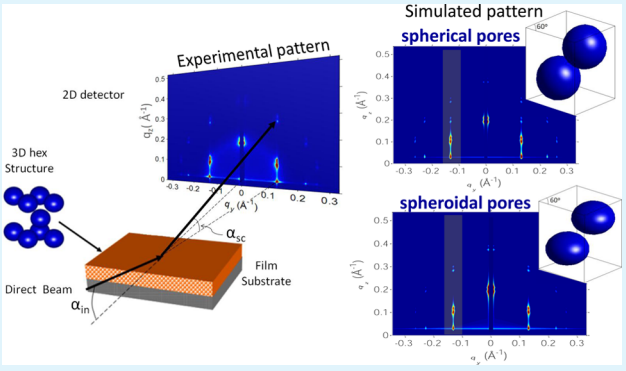

KEYWORDS: *GISAXS, mesoporous silica thin films, deformation of pores, anisotropy*

INTRODUCTION

Mesoscale structures and phenomena are currently among the most intensely studied fields in physics, chemistry, and nanotechnology.[1−5] Being intermediate between the atomic/molecular and macroscopic/continuum length scales, they often require multiscale theories and approaches to be measured and understood. Measuring material samples and devices with mesoscale structures is done using both local probes (scanning tunnelling microscopy (STM), atomic force microscopy (AFM)) and scattering methods such as powder X-ray diffraction (XRD) and transmission electron microscopy (TEM).[6] Structural analysis of mesoscale materials processed to thin films is increasingly carried out by the two surface-sensitive techniques of X-ray reflectivity (XRR) and grazing-incidence small-angle X-ray scattering (GISAXS),[7−9] which have the advantage over TEM of not requiring sample sectioning, which potentially alters the internal structures. In addition, they are excellently suited for in situ studies, since the highly penetrating nature of X-ray beams facilitates the use of bulky sample environments.[10] XRR provides quantitative information about the electron density profile in the direction normal to the surface of the films, through the modeling of specular reflectivity data.[7−9,11−13] GISAXS, which is essentially SAXS applied to surfaces in reflection geometry,[13−20] cf. Figure 1, is complementary to XRR, providing information in the directions both parallel and perpendicular to the thin-film surface, from the diffuse scattering signal. Since the incidence and exit angles involved are small, the usually negligible effects of refraction and multiple scattering should be included for a faithful quantitative modeling of the scattering data. This is difficult, and, in many cases, GISAXS users report only qualitative structural information. A much studied simplified case is that of oriented nanoparticles[21,22] more or less randomly dispersed on a two-dimensional (2D) surface, for which the

Received: November 19, 2013
Accepted: January 17, 2014
Published: January 17, 2014

   dx.doi.org/10.1021/am404602t | ACS Appl. Mater. Interfaces 2014, 6, 2686−2691

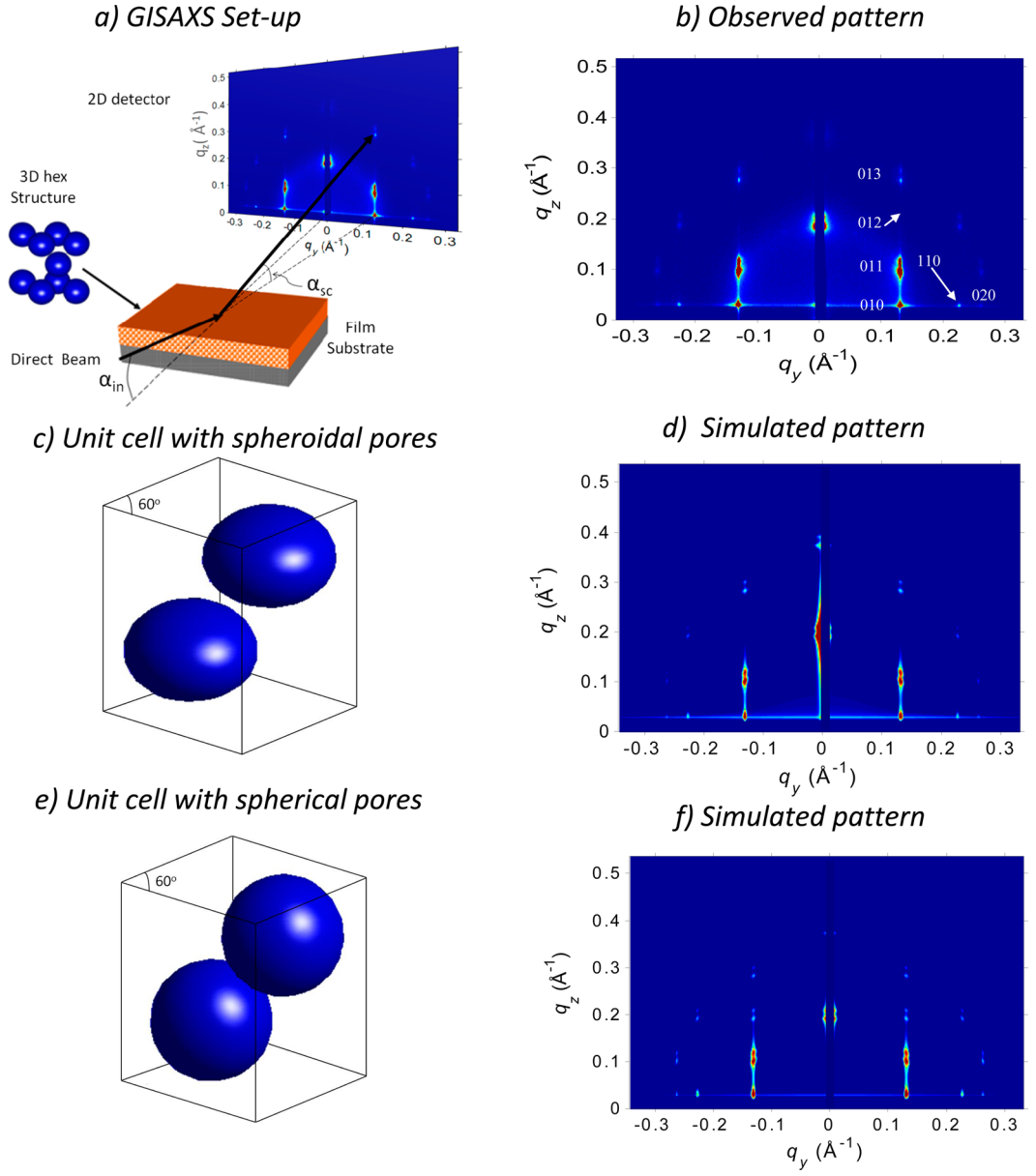

Figure 1. (a) Principle of grazing-incidence small-angle X-ray scattering (GISAXS). The incident monochromatic beam is impinging on the surface of the film at a fixed angle of incidence (α_{in} = 0.13°), and the beam scattered by the scattering objects contained in the film is collected at angles α_{sc} on a 2D detector having the specular direction masked to avoid saturation of the detector. (b) Experimental GISAXS pattern measured on a mesoporous film in which the CTAB surfactant was removed, showing the presence of Bragg reflections characteristic of the $P6_3/mmc$ structure (measurements were made at α_{in} = 0.13°). White arrows indicate two specific reflections that are located essentially at the same wave vector transfer. While the 012 reflection is absent, the 110 reflection is clearly observed, although both are allowed by the space group. (c) Hexagonal unit cell with slightly compressed, i.e., spheroidal, pores used to carry out the simulation R = 2.3 nm and H = 1.85 nm. (d) Simulated GISAXS pattern corresponding to the spheroidal pores shown in panel (c). (e) Hexagonal unit cell with spherical pores R = 2.3 nm. (f) Simulated GISAXS pattern corresponding to the spherical pores shown in panel (e).

computer programs isGISAXS[35] or FitGISAXS[23] are highly adequate. A few researchers[15,18,19,27−31] have also tried to extract more quantitative information from three-dimensional (3D) structures in thin films, but with limited general success, because it is quite challenging to analyze the intensity of Bragg reflections in GISAXS patterns of materials with highly organized porous structures. It seems fair to state that, although GISAXS is a relatively easy technique to apply experimentally, the rather complicated data analysis has impeded GISAXS from becoming a truly widespread technique.

In this work, we show that GISAXS patterns of thin films with ordered internal 3D mesoscale structures can be quantitatively modeled, using the Distorted Wave Born Approximation (DWBA) and related approximations. We go beyond what has previously been achieved in this field by addressing how the anisotropy of the scattering objects can be assessed from a complete fit of the data contained in the GISAXS patterns.

THEORY

In periodic highly organized mesostructured materials, the scattered intensity will tend to be localized to Bragg peaks. As for atomic and molecular crystal structures, the intensity and the location of the Bragg reflections are dependent on the space

dx.doi.org/10.1021/am404602t | ACS Appl. Mater. Interfaces 2014, 6, 2686−2691

group in which the material crystallizes. Contrary to traditional crystallography, however, the repeated scattering objects considered here are on the mesoscale, yielding unit cells with repetition distances with a typical dimension of ~5−20 nm. Another major difference is that, although the atoms in ordinary crystals are usually considered isotropic scatterers, retrieving the anisotropic shape and orientation of the scattering objects is a key objective in the present context.

Since GISAXS is sensitive only to differences in electron density, we base the modeling of scattering from samples exhibiting long-range order on an averaged scattering object shape. Babinet's principle,[32−34] which stipulates that the diffraction patterns of any two complementary objects should essentially be the same, is invoked to calculate the scattering from objects periodically arranged in a host matrix of uniform electron density ρ. From crystallography and the convolution theorem, it follows that the scattering amplitude in q-space, $A(\mathbf{q})$, can be written in the "Born Approximation" (BA) as the sum of a specular and a diffuse term,

$$A(\mathbf{q}) = A_{\text{spec}}(\mathbf{q}) + A_{\text{GISAXS}}(\mathbf{q})$$

where A_{spec} is a function that is nonzero in the specular direction only and describes the amplitude reflected by the flat interfaces of the film (air/film and film/substrate). The GISAXS (diffuse and off-specular) amplitude is given by

$$A(\mathbf{q}) \approx (\rho_{\text{object}} - \rho_{\text{matrix}})P(\mathbf{q})F(\mathbf{q})L(\mathbf{q}) \quad (1)$$

where $(\rho_{\text{object}} - \rho_{\text{matrix}})$ is the contrast of electron density between the repeated object (e.g., micelles or void pores) and the host silica matrix, $P(\mathbf{q})$ the form factor of the pore (micelle), $F(\mathbf{q})$ the structure factor (being the Fourier transform of a single unit cell), and $L(\mathbf{q})$ the Laue function.

Because of the generally anisotropic shape of the scattering objects, all taken to be of the same size and orientation, their form factor $P(\mathbf{q})$ is a function of q rather than q^2. Analytical expressions are tabulated for the form factor of various "standard" shapes, such as cylinders and ellipsoids.[35] (See section 1 and Figure S1 in the Supporting Information for more details.) Notice that the Bragg intensity of all reflections will be strongly modulated by the form factor of these scattering objects. The Laue function is the phase sum over all lattice points within a crystalline region, which for a large crystal approaches a 3D combination of Dirac delta functions located at each node of reciprocal space. In the case of a thin film, the Laue function will present Bragg-rod oscillatory q_z dependence as the film is of finite thickness. The q_z dependence is of particular interest, since it will be affected by refraction effects in the DWBA. For a thin film, the Laue function is thus split into two terms, accounting for the q_z and q_{xy} dependence. Since the characteristic size (ξ) of the in-plane coherent scattering domains is sufficiently large, the Laue function can be replaced by a Gaussian or a pseudo-Voigt in the q_{xy} direction.

The passage from the BA to the DWBA is made by accounting for the refraction correction in the q_z direction, together with the fact that radiation reflected at the film/substrate interface will contribute to the total scattering, yielding to first order in the DWBA four scattering terms.[33,35] Each term corresponds to a specific wave vector q_z inside the film and to different modified amplitudes, as described in the literature by Rauscher et al.[33] and by Lazzari.[35] Finally, an estimate of the GISAXS intensity is obtained by taking the modulus square of the off-specular scattered amplitude, combined with appropriate corrections for instrumental resolution. All the necessary algebra is found in section 2 in the Supporting Information. To simulate the 2D images, the SimDiffraction software[36] was used. This program was originally developed for analyzing textured GIWAXS patterns, and it has been augmented to apply to GISAXS by including the anisotropic form factors of mesoscale scattering objects. The validity of the formalism used in SimDiffraction for the present purposes, effectively taking only the direct and the substrate-reflected beams into account, will be discussed elsewhere.

To demonstrate the usability of our approach, we apply the analysis to a surfactant-templated mesoporous silica film. Hybrid surfactant-templated oxide materials highly organized at the mesoscale have attracted a great deal of attention, since the pioneering work of Kresge et al. in 1992.[1] The main reason for this interest comes from the possibility of producing a highly organized and tailored porosity via removal of the surfactant after calcination,[2] thus opening the route to fabricating mesoporous materials with potential applications such as low-k dielectric materials for electronics,[3] large-surface-area materials for catalysis,[4] or high-efficiency solar cells with mesoporous titania layers.[5] Previous GISAXS studies applied to these materials have allowed the gross structural features to be determined, including the unit-cell parameters and the space group. However, to obtain quantitative information on the geometry of the pores themselves, researchers have relied on sample sectioning, followed by electron microscopy (EM) studies.

RESULTS AND DISCUSSION

The outlined formalism has been applied to a CTAB-templated mesoporous silica thin film produced by evaporation-induced self-assembly.[16] A selected experimental pattern obtained with an incidence angle of 0.13°, chosen slightly above the critical angle of the film to exhibit the full interplay between the DWBA scattering terms, is shown in Figure 1b. The space group of the porous structure in this film is $P6_3/mmc$, colloquially referred to as "hexagonal close packed (HCP)", and there are two micelles per unit cell located at positions $(^1/_3,^2/_3,^1/_4)$ and $(^2/_3,^1/_3,^3/_4)$. The pattern can be indexed according to the given hexagonal space group with lattice parameters a = 5.56 nm and c = 6.97 nm, oriented with the c-axis parallel to the substrate normal. These values are in perfect agreement with those reported by Besson et al.,[37] who first unravelled this structure. The film is composed of crystalline regions which assume random orientations about the surface normal, effectively constituting a "2D powder", as evidenced by the symmetry observed in the experimental patterns. All features seen in the scattering patterns are accounted for by the presented formalism, where in particular the doubling of peaks along the q_z direction can be explained by the application of the DWBA formalism. The doubling of peaks is strongly related to the value of the incident angle, and will vanish under certain conditions, as shown in Figure S3 in the Supporting Information.

Most importantly, the 012 reflection allowed by the space group and shown by an arrow in Figure 1b does not exist, while the 110 reflection that is located at a similar wave vector transfer q from the origin is clearly seen. This rather puzzling observation can be explained by assuming that the pores are not isotropic but rather ellipsoidal in shape, as we shall explain in detail. If a minimum of the form factor coincides with the

location of a Bragg peak, this peak, even if predicted by the space group symmetry, will vanish, as understood from eq 1. The precision with which one can address the disappearance of a Bragg reflection is related to the fact that the micelles being formed by surfactants are highly monodisperse so that their form factors exhibit sharp minima, as discussed by Tate and Hillhouse.[1,26] Gratifyingly, we are able to conclusively confirm the slight out-of-plane compression of the pores previously reported by ellipsometric measurements[38] and EM, relying solely on the GISAXS signal, which opens the path for future in situ studies of the creation and evolution of the porous networks.

The two simulated images differ only by a slight change in the shape of the micelle; Figure 1d is calculated with a spheroidal object (see Figure 1c) in which H = 1.85 nm and R = 2.3 nm; Figure 1f is calculated with a spherical micelle with R = 2.3 nm (see Figure 1e). These two objects are quite similar in shape, but nevertheless the scattering patterns are qualitatively different upon closer investigation. As shown, it is possible to see minute differences in the intensities of the 102 and 110 Bragg reflections, as expected for a change in the anisotropy of the form factor of the pores. Comparing the calculated patterns to the experimental one (shown in Figure 1a), it is clear that the best agreement corresponds to the simulation of Figure 1c. This shows unambiguously that a distortion as small as H/R = 0.8 of the sphere, corresponding to a change in radius of 0.45 nm, is measurable. The excellent quantitative agreement is further highlighted by refining extracted lines of intensity along the q_z and q_y directions, as shown in Figure 2, clearly demonstrating the feasibility of quantitative analysis of GISAXS patterns from 3D mesoscale structures. For an even better description of the intensity, we have included in these simulations two additional contributions of diffuse scattering. One of them arises from a minor fraction of the film volume having a disordered "wormlike" structure. It is located on a ring of constant q and appears at the outer tail of the 010 reflection. The second one is due to scattering by the beam-defining slits having a very narrow aperture (20 μm). This streak gives rise to scattering located along the Yoneda line in the q_{xy} scan of Figure 2 going from −0.2 Å^{-1} to 0.2 Å^{-1}. We can extract from this calculation all the parameters reported in Table 1. Not only does the simulation provide the space group and the lattice parameters, but also the anisotropy of the pores and the size of the domains which scatter coherently in the plane of the film. Thus, by looking at the intensity of symmetry-allowed Bragg reflections, we can probe the anisotropic shape of the pores. Specifically, we take advantage of the observation that some reflections that are allowed by the space group vanish, while others located at the same wave vector transfer remain observable. It is remarkable that measuring zero intensity at given locations is a key to determine the anisotropic shape of the scattering objects.

This specific example of a $P6_3/mmc$ mesoporous silica structure was chosen to illustrate the capabilities of our approach to simulate GISAXS patterns; further examples are discussed in the Supporting Information.

CONCLUSION

We have outlined a general and versatile method based on the use of the DWBA and related approximations, as described in detail in the Supporting Information (section S2), with analytical expressions for calculating the GISAXS patterns of any mesoscopically ordered periodic structure in thin films.

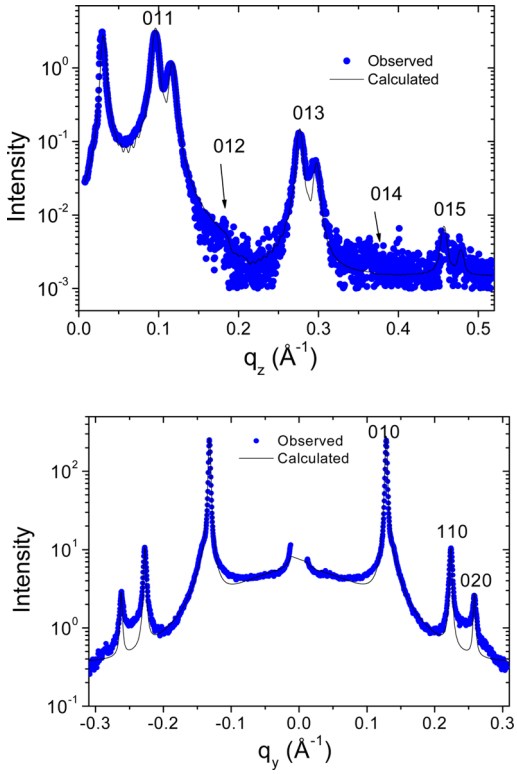

Figure 2. Fitted scans along the q_z (cut along q_y = 0.132 Å^{-1}) and q_{xy} (cut along q_z = 0.116 Å^{-1}) directions according to the formalism presented in the text. In this case, the scan along the q_y direction was calculated by adding a central background and a peaked background at q_{xy} = 0.135 Å^{-1} to account for the existence of a shoulder on the right side of the first Bragg peak. This shoulder is consistent with the existence of a fine diffuse halo seen in the GISAXS pattern which might come from the presence of "wormlike" domains in the film. The GISAXS pattern was measured at an incidence angle of 0.13°. For the q_z scan the doubling of the peaks is due to the different terms included in the DWBA, which take in account the reflection of X-rays on the substrate before and after scattering by the pores.

Table 1. Refined Parameters Used in the Fit to the Data of the q_{xy} and q_z Scans Shown in Figure 2

parameter	value
lattice parameters	
a	5.56 nm
c	6.97 nm
pore radius in the plane of the substrate, R	2.3 nm
pore radius perpendicular to the substrate, H	1.85 nm
in-plane correlation length, ξ (nm)	1500 nm
critical angle of the film, α_{cfilm}	0.108°
absorption of the film, β_{film}	0.2×10^{-7}
roughness of the surface, σ	0.3 nm
number of pore layers, N_z	13

This approach yields excellent quantitative fits to the experimental intensities of the Bragg reflections measured in the GISAXS patterns. In this respect, the present analysis provides unprecedented access to the anisotropy of scattering objects, such as pores. Our approach can be generalized to extract quantitative information from GISAXS patterns of any 3D ordered structure (cf. Figure S4 in the Supporting Information) including not only micelles and block copolymer liquid-crystalline phases, but also core/shell nanoparticle

superstructures, ordered nanocomposites, and any crystalline mesoporous materials deposited on a substrate, thus further substantiating the claim of GISAXS as the method of choice for studying nanoscale and mesoscale thin-film assemblies.

METHODS

GISAXS Experiments. Films were initially characterized by GISAXS on the Rigaku GISAXS setup of IMMM and later on at ESRF on Beamline ID02 at fixed energy and different angles of incidence. GISAXS is a special technique widely used to measure the scattering of nanosized objects at surfaces. It consists of shining an X-ray beam at a fixed angle of incidence and collecting the scattered intensity on a 2D detector located at a distance of the order of 1 m from the sample. The direction which corresponds to specular reflection on the film is generally masked to avoid saturation and damage of the detector (see Figure 1a). The scattering vector $\mathbf{q}$ is the difference between the incoming and outgoing wavevectors, $\mathbf{q} \equiv \mathbf{k}_f - \mathbf{k}_i$, which in the case of cylinder symmetry is most conveniently decomposed into in-plane and out-of-plane components q_{xy} and q_z. The modulus is given by $q = 4\pi \sin(\theta)/\lambda$. Since GISAXS measurements are carried out in the small-angle regime, Lorentz and polarization corrections are negligible.

The experimental conditions for GISAXS measurements made at IMMM include the following: fixed angle of incidence ($\alpha_i = 0.15°$, using an exposure time of 3600 s). The incident beam was set to a size of 200 μm × 200 μm after being reflected and monochromatized (λ = 0.154 nm) on an Osmic mirror. A series of three consecutive pinholes was used for collimation. The beam was produced by a copper rotating anode working at 45 kV and 50 mA. The scattering pattern was recorded on a wire detector (Gabriel type) located at 83 cm from the sample with a pixel size of 150 μm. The entire flight path of the beam was evacuated to reduce stray scattering and beam damage.

The experimental conditions for measurements made at ID02 ESRF include the following: angle of incidence varies ($\alpha_{in} = 0.05°–0.14°$, using an exposure time of 10 s per frame). The incident monochromatic beam (λ = 0.0998 nm) was set to a size of 20 μm × 50 μm. The scattering pattern was recorded on a 2D CCD detector (FReLoN, ESRF) located 100 cm from the sample with a pixel size of 52 μm. The entire flight path of the beam was evacuated.

Mesoporous Thin Films. The mesoporous silica thin film investigated in this study was produced using the concept of Evaporation Induced Self-Assembly (EISA), in which micelles of a surfactant are used to template silica. CTAB-templated silica thin films were synthesized by dip-coating a silicon wafer from an initial sol prepared in two steps, following previously reported procedures.[6,39] A prehydrolyzed solution was first prepared by refluxing tetraethoxysilane TEOS), Millipore water, and hydrochloric acid for 1 h. Then, a second solution, prepared by dissolving the surfactant in ethanol (under acidic conditions) was added to the hydrolyzed one. The film was templated by CTAB with a final solution of TEOS:C_2H_5OH:HCl:H_2O:CTAB molar composition of 1:20:0.004:4:0.10. Such a composition is known to yield films having $P6_3/mmc$ symmetry, as is confirmed by GISAXS. Final sols were aged for 4 days. In order to make very thin films, the sol was further diluted by adding 21 g of ethanol, and the films were dip-coated at a constant withdrawal velocity of 3.6 cm/min on a silicon substrate. (The surfactant was eventually removed by rinsing the films in a solution containing ethanol and hydrochloric acid with a C_2H_5OH:HCl molar ratio of 1:0.007 for 90 min at a temperature of T = 60 °C.)

ASSOCIATED CONTENT

Supporting Information

Detailed description of form factors, DWBA formalism for ordered mesostructured materials, dependence on incidence angle (peak doubling) and fitted examples. This material is available free of charge via the Internet at http://pubs.acs.org.

AUTHOR INFORMATION

Corresponding Authors

*E-mail: dag.breiby@ntnu.no (D.W.B.).
*E-mail: gibaud@univ-lemans.fr (A.G.).

Notes

The authors declare no competing financial interest.

ACKNOWLEDGMENTS

This work was supported by the French–Norwegian program Aurora and the Protea program. We thank the Région des Pays de la Loire for financial support in funding the GISAXS instrument at Université du Maine (Le Mans) and the Ph.D. thesis of Elvia Chavez. We are also greatly indebted to the ESRF for supporting the Ph.D. studies of Elvia Chavez and for giving us access to the ID02 and ID10 beamlines and NSLS for access to the X22B beamline.

REFERENCES

(1) Kresge, C.; Leonowicz, M.; Roth, W.; Vartuli, J.; Beck, J. *Nature* **1992**, *359*, 710.
(2) Sanchez, C.; Boissière, C.; Grosso, D.; Laberty, C.; Nicole, L. *Chem. Mater.* **2008**, *20*, 682–737.
(3) Saxena, R.; Rodriguez, O.; Cho, W.; Gill, W.; Plawsky, J.; Baklanov, M.; Mogilnikov, K. *J. Non-Cryst. Solids* **2004**, *349*, 189.
(4) Trong On, D.; Desplantier-Giscard, D.; Danumah, C.; Kaliaguine, S. *Appl. Catal., A* **2001**, *222*, 299–357.
(5) Zukalová, M.; Zukal, A.; Kavan, L.; Nazeeruddin, M.; Liska, P.; Grätzel, M. *Nano Lett.* **2005**, *5* (9), 1789.
(6) Zhao, D.; Feng, J.; Huo, Q.; Melosh, N.; Fredrickson, G.; Chmelka, B.; Stucky, G. *Science* **1998**, *279*, 548–552.
(7) Gibaud, A.; Dourdain, S.; Vignaud, G. *Appl. Surf. Sci.* **2006**, *253* (1), 3.
(8) Dourdain, S.; Bardeau, J.-F.; Colas, M.; Smarsly, B.; Mehdi, A.; Ocko, B.; Gibaud, A. *Appl. Phys. Lett.* **2005**, *86*, 113108-1–113108-3.
(9) Dourdain, S.; Gibaud, A. *Appl. Phys. Lett.* **2005**, *87*, 223105.
(10) Esmaeili, M.; Fløystad, J.; Diaz, A.; Høydalsvik, K.; Guizar-Sicairos, M.; Andreasen, J.; Breiby, D. *Macromolecules* **2013**, *46*, 434–439.
(11) Dourdain, S.; Britton, D.; Reichert, H.; Gibaud, A. *Appl. Phys. Lett.* **2008**, *93*, 183108.
(12) Gibaud, A.; Baptiste, A.; Doshi, D.; Brinker, C.; Yang, L.; Ocko, B. *Europhys. Lett.* **2003**, *63*, 833–839.
(13) Besson, S.; Gacoin, T.; Ricolleau, C.; Jacquiod, C.; Boilot, J. *J. Mater. Chem.* **2003**, *13*, 404–409.
(14) Besson, S.; Gacoin, T.; Jacquiod, C.; Ricolleau, C.; Babonneau, D.; Boilot, J. *J. Mater. Chem.* **2000**, *10*, 1331–1336.
(15) Smarsly, B.; Gibaud, A.; Ruland, W.; Sturmayr, D.; Brinker, C. *Langmuir* **2005**, *21*, 3858–3866.
(16) Doshi, D.; Gibaud, A.; Goletto, V.; Lu, M.; Gerung, H.; Ocko, B.; Han, S.; Brinker, C. *J. Am. Chem. Soc.* **2003**, *125*, 11646.
(17) Grosso, D.; Cagnol, F.; Soler-Illia, G.; Crepaldi, E.; Amenitsch, H.; Brunet-Bruneau, A.; Bourgeois, A.; Sanchez, C. *Adv. Funct. Mater.* **2004**, *14*, 309–322.
(18) Altamura, D.; Holý, V.; Siliqi, D.; Lekshmi, I.; Nobile, C.; Maruccio, G.; Cozzoli, P.; Fan, L.; Gozzo, F.; Giannini, C. *Cryst. Growth Des.* **2012**, *12*, 5505–5512.
(19) Buljan, M.; Radic, N.; Bernstorff, S.; Drazic, G.; Bogdanovic-Radovic, I.; Holý, V. *Acta Crystallogr., Sect. A: Found Crystallogr.* **2012**, *A68*, 124–138.
(20) Pietra, F.; Rabouw, F.; Evers, W.; Byelov, D.; Petukhov, A.; Donegá, C.; Vanmaekelbergh, D. *Nano Lett.* **2012**, *12*, 5515–5523.
(21) Renaud, G.; Lazzari, R.; Revenant, C.; Barbier, A.; Noblet, M.; Ulrich, O.; Leroy, F.; Jupille, J.; Borensztein, Y.; Henry, C.; Deville, J.; Scheurer, F.; Mane-Mane, J.; Fruchart, O. *Science* **2003**, *300*, 1416–1420.
(22) Breiby, D.; Chin, P.; Andreasen, J.; Grimsrud, K.; Di, Z.; Janssen, R. *Langmuir* **2009**, *25*, 10970–10974.

(23) Babonneau, D. J. *J. Appl. Crystallogr.* **2010**, *43*, 929−936.
(24) Förster, S.; Timmann, A.; Konrad, M.; Schellbach, C.; Meyer, A.; Funari, S. S.; Mulvaney, P.; Knott, R. *J. Phys. Chem. B.* **2005**, *109*, 1347−1360.
(25) Smilgies, D. M.; Blasini, D. R. *J. Appl. Crystallogr.* **2007**, *40*, 716−718.
(26) Tate, M. P.; Hillhouse, H. W. *J. Phys. Chem. C* **2007**, *111*, 7645−7654.
(27) Smilgies, D.; Heitsch, A.; Korgel, B. *J. Phys. Chem. B* **2012**, *116*, 6017−6026.
(28) Senesi, A.; Eichelsdoerfer, D.; Macfarlane, R.; Jones, M.; Auyeung, E.; Lee, B.; Mirkin, C. *Angew. Chem., Int. Ed.* **2013**, *52*, 6624−6628.
(29) Lee, B.; Park, I.; Yoon, J.; Park, S.; Kim, J.; Kim, K.; Chang, T.; Ree, M. *Macromolecules* **2005**, *38*, 4311−4323.
(30) Busch, P.; Rauscher, M.; Smilgies, D.; Posselt, D.; Papadakis, C. *J. Appl. Crystallogr.* **2006**, *39*, 433−442.
(31) Stein, G.; Kramer, E.; Li, X.; Wang, J. *Macromolecules* **2007**, *40*, 2453−2460.
(32) Jackson, J. D. *Classical Electrodynamics*, 3rd Edition; John Wiley & Sons: New York, 1999.
(33) Rauscher, M.; Salditt, T.; Spohn, H. *Phys. Rev. B* **1995**, *52* (23), 16855−16863.
(34) Du, P.; Li, M.; Douki, K.; Li, X.; Garcia, C.; Jain, A.; Smilgies, D.; Fetters, L.; Gruner, S.; Wiesner, U.; Ober, C. *Adv. Mater.* **2004**, *16*, 953−957.
(35) Lazzari, R. *J. Appl. Crystallogr.* **2002**, *35*, 406−421.
(36) Breiby, D.; Bunk, O.; Andreasen, J.; Lemke, H.; Nielsen, M. *J. Appl. Crystallogr.* **2008**, *41*, 262−271.
(37) Besson, S.; Ricolleau, C.; Gacoin, T.; Jacquiod, C.; Boilot, J. *J. Phys. Chem. B* **2000**, *104*, 12095−12097.
(38) Boissiere, C.; Grosso, D.; Lepoutre, S.; Nicole, L.; Bruneau, A.; Sanchez, C. *Langmuir* **2005**, *21*, 12362−12371.
(39) Tate, M. P.; Urade, V.; Kowalski, J.; Wei, T.; Hamilton, B.; Eggiman, B.; Hillhouse, H. *J. Phys. Chem. B* **2006**, *110*, 9882−9892.